Visualising G-quadruplex DNA dynamics in live cells by fluorescence lifetime imaging microscopy

Peter A. Summers,[1] Ben Lewis,[1,2,3] Jorge Gonzalez-Garcia,[1,6] Aaron H.M. Lim,[1] Paolo Cadinu,[1] Rosa M. Porreca,[2,3] Nerea Martin-Pintado,[4] David Mann,[5] Joshua B. Edel,[1] Jean Baptiste Vannier,[2,3]* Marina K. Kuimova,[1]* Ramon Vilar[1]*

Addresses:

[1] Department of Chemistry, Molecular Sciences Research Hub, White City Campus, Imperial College London, W12 0BZ, UK.

[2] Telomere Replication and Stability group, Medical Research Council – London Institute of Medical Sciences, London, W12 0NN, UK.

[3] Institute of Clinical Sciences, Faculty of Medicine, Imperial College London, London, W12 0NN, UK.

[4] Oncode Institute, Hubrecht Institute–KNAW and University Medical Center Utrecht, Utrecht, The Netherlands.

[5] Department of Life Sciences, Imperial College London South Kensington, London, SW7 2AZ, UK.

[6] Current address: Department of Inorganic Chemistry, University of Valencia, Jose Beltran 2, Paterna, 46980, Spain.

Corresponding authors:

Prof Ramon Vilar; r.vilar@imperial.ac.uk; tel +44 (0)20 7594 1967

Dr Marina K Kuimova; m.kuimova@imperial.ac.uk; tel +44 (0)20 7594 8558

Dr Jean-Baptists Vannier; j.vannier@imperial.ac.uk; tel +44 (0)20 3313 4155

ABSTRACT

Guanine rich regions of oligonucleotides fold into quadruple-stranded structures called G-quadruplexes (G4). Increasing evidence suggests that these G4 structures form *in vivo* with a crucial role in cellular processes, however, their direct observation in live cells remains a challenge. Here we unequivocally demonstrate that a fluorescent probe (**DAOTA-M2**) in conjunction with Fluorescence Lifetime Imaging Microscopy (FLIM) can identify G4 within nuclei of live and fixed cells. We have developed a new FLIM-based cellular assay to study the interaction of non-fluorescent small molecules with G4, which can be applied to a wide range of drug candidates. We demonstrate that **DAOTA-M2** can be used to study G4 stability in live cells. Disruption of *FancJ* DNA helicase activity increases G4 lifetime, directly establishing for the first time its biological activity in mammalian cells.

INTRODUCTION

Guanine-rich sequences of DNA can fold into tetra-stranded helical assemblies known as G-quadruplexes (G4). These structures have been implicated in a number of essential biological processes such as telomere maintenance, transcription, translation and replication.[1-4] A series of bioinformatical studies initially suggested that there are over 350,000 putative G4-forming sequences in the human genome,[5,6] with subsequent studies reporting an even larger number.[7] Following these predictions, sequencing studies using purified human genomic DNA revealed over 700,000 sequences that form G4 structures under *in vitro* conditions.[8] More recently, the prevalence of G4s in human chromatin have been investigated using an immunoprecipitation technique.[9,10] These studies showed that there are over 10,000 sequences in the human genome that can form G4 DNA structures under cellular conditions.[9] Interestingly, these G4 structures are mainly located in gene promoter regions and in 5'-untranslated regions (5'-UTR) of genes supporting the proposed hypothesis that G4 DNA is involved in a number of essential biological regulatory processes.

While the exact roles that G4 structures play in biology are still under significant scrutiny, it is commonly accepted that G4 formation can be detrimental to certain biological processes and can lead to DNA damage.[11,12] Therefore, it is not surprising that several helicases such as *Pif1*, *RecQ*, *RTel1*, *FancJ* and *BLM* have been found to unfold G4 structures *in vitro*.[13] While it is known that G4 DNA helicases are important in maintaining genome integrity in cells, the direct link between their *in vitro* G4 unwinding activity and genome instability associated with their mutations is still missing.

Considering the wide range of biological processes associated with G4s, there has been significant interest in developing tools to detect and visualise G4 DNA structures in cells. With exceptional affinity and widespread application in immunofluorescent staining, high-affinity antibodies have been developed to visualise G4 in cells.[14-18] An early antibody found to be

selective against telomeric G4 showed nuclear staining in the ciliate *Stylonychia lemnae*.[15] Subsequent studies have reported high-affinity antibodies able to visualise G4 DNA and G4 RNA in mammalian cells by immunofluorescent staining.[16-18] While these elegant studies are the most direct evidence of the presence of G4 DNA structures in cells, they have a number of potential drawbacks. The fixation process can denature the cellular DNA and induce DNA degradation,[19,20] and the high affinity of the antibodies for G4 could artificially increase the presence of G4 structures. Furthermore, antibodies are not suitable for use in live cells and hence cannot be used to study G4 dynamics in real time.

These limitations can be overcome by using small-molecule optical probes.[21-23] However, most G4 DNA optical probes rely on a large enhancement in emission intensity upon binding G4 ('switch-on'), compared to binding duplex (ds) DNA.[23] For example, Thioflavin T (ThT) and its derivatives have shown to be switch-on probes for G4 DNA, with up to 150-fold fluorescence enhancement *vs.* dsDNA (under optimal conditions) and have been used for live cell imaging of both DNA and RNA G4.[24-26] However, ThT is known to bind to other biologically relevant molecules (*e.g.* protein aggregates[27]) and is highly sensitive to the matrix microviscosity,[28] potentially triggering non-G4 emission. While these small molecule probes provide a good way of studying G4s in cell-free environments, their emission intensity is concentration dependent. In the vast excess of nuclear dsDNA (and other biomolecules), distinguishing G4 *foci* from background emission is challenging, even with a very high switch on ability. Additionally, quantifying the emission intensity is not possible when the cellular concentration of neither the probe nor G4s are known.

An alternative approach is to use a change in the fluorescence lifetime (a concentration-independent parameter) of a probe upon binding to different DNA structures.[29-33] For example, the fluorescence lifetime of 3,6-bis(1-methyl-2-vinyl-pyridinium) carbazole diiodide (o-BMVC) is longer when bound to G4 (*ca.* 2.5 ns) than non G4 DNA sequences (*ca.* 1.5 ns).

This difference was used to identify long lifetime *foci* in both the nucleus and cytoplasm of mammalian cells, however, this dye is only permeable to fixed cells and so no dynamic live cell work was possible.[31,32] More recently, a fluorescence lifetime-based probe (a tripodal cationic fluorescent molecule, NBTE) was reported that can distinguish G4 (3-4 ns) and dsDNA (2.0-2.5 ns) in live cells.[33] We previously reported that **DAOTA-M2** [Figure 1(a)] has a remarkably different fluorescence lifetime when bound to G4 structures as compared to duplex or single-stranded DNA, with good live cell permeability and low cytotoxicity.[30] Herein we show that **DAOTA-M2** can be uniquely used to visualise dynamic processes involving G4 in live cells. We confirm that while the probe works in fixed cells, there are differences in G4 abundance, highlighting the importance of carrying out G4 imaging experiments in live, rather than fixed environments. We demonstrate that **DAOTA-M2** can be used to separate the molecular functions of DNA helicase *FancJ* involved in genome stability and the distribution of G4 in live cells. By disturbing the activity of *FancJ* in mammalian cells, we provide the first direct evidence of its ability to resolve G4 DNA in live cells. Finally, we have developed a new quantitative fluorescence lifetime-based assay to visualise the strength and the rates of interaction of small molecules (which are not fluorescent themselves) with G4 in live cells.
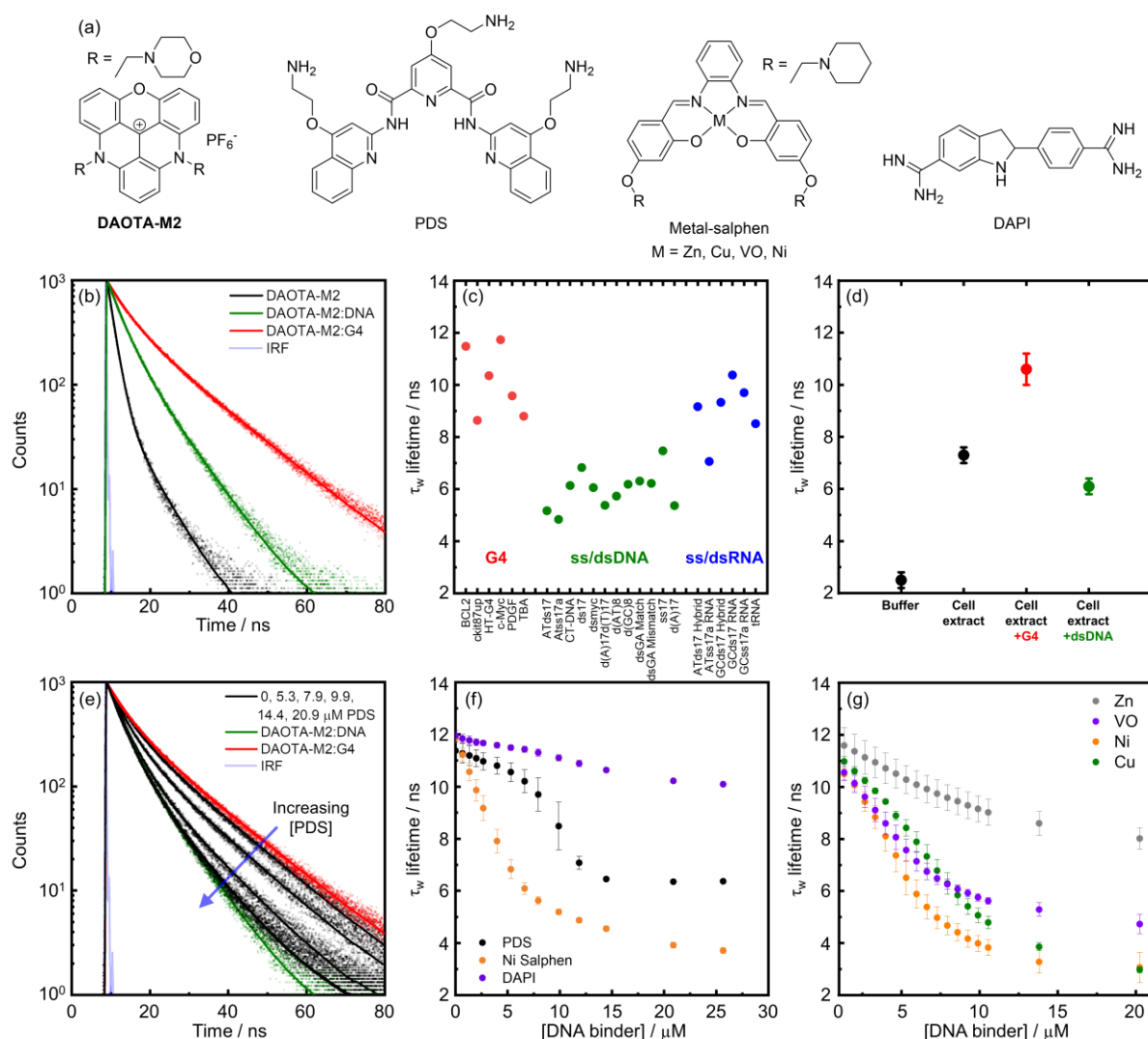
Figure 1. *In vitro* fluorescence-lifetime of **DAOTA-M2** bound to different DNA topologies. (a) Chemical structures of the DNA binders under study in this work. (b) Time resolved fluorescence decays of **DAOTA-M2** (2 µM, black trace) and following the subsequent additions of dsDNA (CT-DNA, 20 µM, green trace) and then G4 (*c-Myc*, 4 µM, red trace). (c) Variation of the average lifetime (τ_w) of **DAOTA-M2** in the presence of different G4 (red dots), ss/dsDNA (green dots) and ss/dsRNA (blue dots), adapted from reference [30]. (d) Fluorescence-lifetimes of **DAOTA-M2** (2 µM) in aqueous buffer, buffered *Xenopus* egg extract (33 µL egg extract + 12 µL aqueous buffer), and in buffered cell extract supplemented with G4 (4 µM *c-Myc*) and dsDNA (44 µM ds26). Both measurements remained constant over 0.5 hr incubation at 21 °C. (e) In a mixture of **DAOTA-M2** (2 µM), dsDNA (CT-DNA, 20 µM) and G4 (*c-Myc*, 4 µM), increasing amounts of PDS (5.3. 7.9. 9.9 and 14.4 µM, black traces) displaces **DAOTA-M2** from a G4 to dsDNA environment. (f) Variation of τ_w in a mixture of **DAOTA-M2** (2 µM), dsDNA (CT-DNA, 20 µM), and G4 (*c-Myc*, 4 µM), with increasing concentrations of G4 binders PDS (black dots) and Ni-salphen (orange dots), and a non-G4 binder DAPI (purple dots). See Figure S2 for example decays. (g) Variation of τ_w in a mixture of **DAOTA-M2** (2 µM) and G4 (*c-Myc*, 4 µM), with increasing concentrations of Zn (grey dots), VO (purple dots), Ni (orange dots) and Cu (green dots) salphens. Error bars are ± standard deviation of three repeats. In less stated otherwise, all experiments in 10 mM lithium cacodylate buffer (pH 7.3) with 100 mM KCl.

RESULTS

In vitro **characterisation of DAOTA-M2 interacting with G4 and dsDNA in** *Xenopus* **egg extract and buffered solutions.** Previously, we have shown that **DAOTA-M2** is a medium-strength DNA binder,[34] with a moderately greater affinity for G4 over dsDNA (K_d = *ca.* 1.7 µM for dsDNA and *ca.* 1.0 µM for G4).[30,35] Despite similar binding affinities, the mean weighted average lifetime (τ_w) upon binding is found to be highly dependent on the DNA topology. These values range from *ca.* 5 – 7 ns when bound to dsDNA, *ca.* 7 – 11 ns when bound to RNA and *ca.* 9 – 12 ns when bound to G4 DNA [Figure 1(b) and (c)] and are independent of absolute concentration [Figure S1(a)]. Given the complex excited state decay of **DAOTA-M2**, we have now optimised our fitting algorithm and have chosen to use τ_w as a reporter instead of τ_2 as used previously, due to a more straightforward and accurate fitting of fluorescence lifetime imaging data (*vide infra*).[30]

To establish the effect of proteins, lipids, carbohydrates and biomolecules other than nucleic acids on the lifetime of **DAOTA-M2**, we used a highly protein-concentrated and nucleic acid-depleted Xenopus egg extract.[36] τ_w increases from 2.5 ± 0.3 ns in aqueous buffer to 7.3 ± 0.3 ns in cell extract [Figure 1(d)], indicating an effect from other biomolecules on the fluorescence lifetime. Reassuringly, τ_w increases to 10.6 ± 0.6 ns on addition of G4 to the extract, and decreases to 6.1 ± 0.3 ns with dsDNA, consistent with the results observed in aqueous buffered solutions [Figure 1(c)]. This result implies a higher affinity of **DAOTA-M2** for DNA over other cellular biomolecules. In a nuclear environment, given the vast excess of nucleic acid, **DAOTA-M2** should preferentially bind to DNA and the lifetime will give an indication of the DNA topology.

We next set out to examine whether the **DAOTA-M2** lifetime can report on competitive interactions of other binders to G4 *in vitro*. Due to a higher affinity for G4, addition of G4 to a mixture of **DAOTA-M2** and dsDNA increases the lifetime from 6.1 ± 0.2 ns [Figure 1(e),

green trace] to 11.7 ± 0.4 ns [Figure 1(e), red trace]. The subsequent addition of pyridostatin (PDS), a highly specific G4 binder with a greater affinity for G4 than **DAOTA-M2** ($K_d = ca.\ 0.5$[37,38] and $ca.\ 1.0\ \mu M$[30], respectively), displaces **DAOTA-M2** from G4 back to dsDNA, accompanied by a drop in τ_w [Figure 1(f), black dots]. When the experiment is repeated using DAPI, which is a well-established dsDNA minor groove binder[39] and non-G4 binder, only a small drop in τ_w is observed as **DAOTA-M2** stays bound to G4 [Figure 1(f), purple dots]. The dynamic equilibrium between dsDNA and G4 bound **DAOTA-M2** can also be disrupted through the addition of a large excess of dsDNA into a solution of G4 and **DAOTA-M2** [Figure S1(b)].

We then investigated **DAOTA-M2** displacement using Ni-salphen, another G4 binder which has a higher affinity for both G4 and dsDNA than **DAOTA-M2** [Figure S1(c)]. [40,41] In this case τ_w drops below the region associated with dsDNA to $ca.\ 3.7$ ns, close to that of free dye [Figure 1(f), orange dots]. A range of metal-salphen complexes (with metal = Ni, Cu, VO, Zn) are an ideal series to study structurally related molecules with different G4 affinities, as variation in the metal centre changes the metal coordination geometry, which has a dramatic effect on G4 binding: strong (Ni, Cu), medium (VO) and weak (Zn).[42,43] Our **DAOTA-M2** lifetime-based data [Figure 1(g)] confirmed this previoulsy reported binding trend[43] of the four complexes.

It appears from our data that in mixtures of G4 and dsDNA, analysis of the **DAOTA-M2** lifetime can accurately differentiate between distinct DNA topologies, thus, we next looked to investigate **DAOTA-M2** in live cells using fluorescence lifetime imaging microscopy (FLIM).
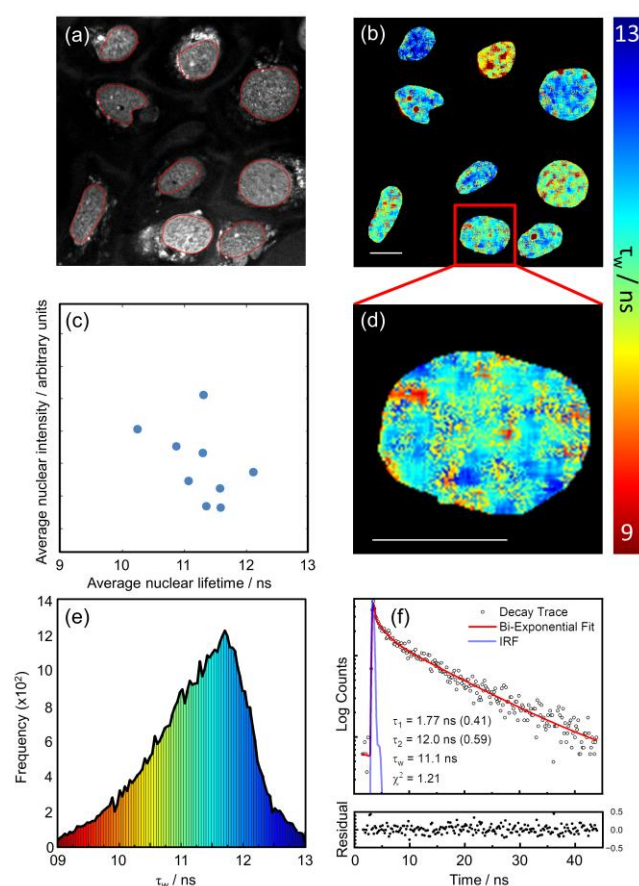
Figure 2. FLIM analysis of nuclear DNA in live U2OS cells stained with **DAOTA-M2** (20 μM, 24 h). (a) Fluorescence intensity image recorded at 512 x 512 resolution (λ_{ex} = 477 nm, λ_{em} = 550-700 nm), red lines represent the nuclear segmentation used for the FLIM analysis. (b) FLIM map from (a). (c) 2D correlation of the average nuclear intensity against the average nuclear lifetimes in (b). (c) Zoomed in nucleus from (b). (e) Histogram of fluorescence lifetime distribution in (b). (f) fluorescence decay, fit, and normalised residual of a representative pixel (including binning) in (b). Scale bars: 20 μm.

Imaging G4s *in cellulo* using DAOTA-M2 and FLIM. Given the *in vitro* assay results [Figure 1] confirming that **DAOTA-M2** lifetime can predict the strength of interaction between small molecule binders and G4s, we set out to use **DAOTA-M2** to study the interaction of any molecule with G4s in live cells [Figures 2 and 3].

We were able to record FLIM images at high magnification, making it possible to visualise spatial lifetime distributions within the nucleus [Figure 2(d)]. Consistent with *in vitro* experiments, fluorescence decays were fitted to a bi-exponential decay model [Figure 2(f)] to obtain the corresponding fluorescence lifetimes (τ_w). Figures 2(b) and (d) show resulting FLIM maps; each cell nucleus displays spatially heterogenous lifetime distributions, with areas

corresponding to long (12-13 ns, blue) and short (9-10 ns, red) lifetimes. Taking an average τ_w of each cell nucleus, nuclear lifetimes fall in a 10-12 ns range and are not correlated with intensity [Figure 2(c)], indicative of the absence of self-quenching. Importantly, increasing dye uptake (and therefore fluorescence intensity) through incubation in starvation conditions results in a minimal change in nuclear lifetimes [Figure S3], confirming the concentration independence of the FLIM measurement.

We then employed the same *in vitro* displacement assay [Figure 1(f)] for *in cellulo* studies using PDS and DAPI. Co-incubation with **DAOTA-M2** (20 µM) and PDS for 24 h results in remarkably different cellular lifetimes, dropping from 11.4 ± 1.0 ns in control cells to 10.3 ± 1.8 ns (5 µM PDS) and 9.0 ± 1.3 ns (10 µM PDS) [Figure 3(b)]. The smaller drop in τ_w with a lower PDS concentration confirms the high concentration of PDS needed to disturb the equilibrium between **DAOTA-M2** and G4, seen above *in vitro* [Figure 1(f)]. As a negative control, incubation with DAPI (25 and 50 mM, 1 h) led to no change in the average nuclear lifetimes [Figure 3(b)], with nuclear localisation confirmed from the DAPI emission [Figure S4]. Based on consistency of these results with the *in vitro* characterisation [Figure 1] and previous cellular work using **DAOTA-M2** with PDS,[30] we hypothesise that the lifetime drop *in cellulo* is the result of nuclear displacement of **DAOTA-M2** from G4.

PDS (as well as many other G4 binders, including the metal-salphen complexes discussed below[40]) is known to cause DNA damage and arrest cell growth,[44] evident in the brightfield images before and after incubation with PDS [Figure S5(b)]. As a control, we ran an experiment in the presence of cisplatin, known to form DNA intra-strand links and activate the apoptotic pathway.[45] In this experiment, a slight increase in the nuclear lifetime of **DAOTA-M2** was observed [Figure S5(a)], excluding DNA damage as the cause of the lifetime decrease observed after incubation with PDS.

FLIM studies using fixed cells. It is common for immunostaining or small molecule staining of G4 in cells to be performed following PFA fixation (needed for permeabilising the cellular membrane), which crosslinks proteins, increases cell rigidity and chemically alters the cell morphology. This process is known to impact nucleic acids within the cell, denaturing DNA and causing DNA damage.[19,20] However, DNAse and RNAse treatment is possible in fixed cells, and allows for examination of the effect of nuclear RNA on the **DAOTA-M2** lifetime. This is an important control given the overlap in lifetimes when **DAOTA-M2** is bound to G4 structures and non-G4 RNA [Figure 1(c)].

Fixing with 4% PFA results in a drop in average τ_w by *ca.* 1 ns to 10.6 ± 1.1 ns, an interesting result as it implies that the DNA topology has been disrupted during fixation [Figure 3(d)]. Reassuringly, addition of PDS (10 µM, 1 hr) has the same response as in live cells, with τ_w dropping to mean $= 9.1 \pm 1.4$ ns and median $= 8.5 \pm 1.4$ ns. In this experiment, the bi-modal distribution (formed due to limited PDS uptake by some cells) is best represented using the median. Treatment of fixed cells with RNAse has no effect on the average τ_w, confirming that RNA in the cell nucleus does not affect **DAOTA-M2** lifetime. DNAse treatment, however, did result in a drop in nuclear lifetime to 9.3 ± 0.9 ns. This value falls in-between that of **DAOTA-M2** bound to dsDNA (median $= 8.5 \pm 1.4$ ns) and in a mixture of dsDNA/G4 (10.6 ± 1.1 ns in fixed cells). This pattern is replicated in the *Xenopus* egg extract experiment above [Figure 1(d)].

Thus, our fixed cell experiments confirm that nuclear RNA does not contribute to the high **DAOTA-M2** lifetime observed in cells, and therefore this lifetime can be attributed to G4 DNA structure formation. At the same time our data seem to indicate that more G4s are stained by **DAOTA-M2** in live rather than in fixed cells (all of which are being equally displaced by PDS), although the effect of fixation on other cellular components and its knock-on effect on **DAOTA-M2** binding cannot be excluded.
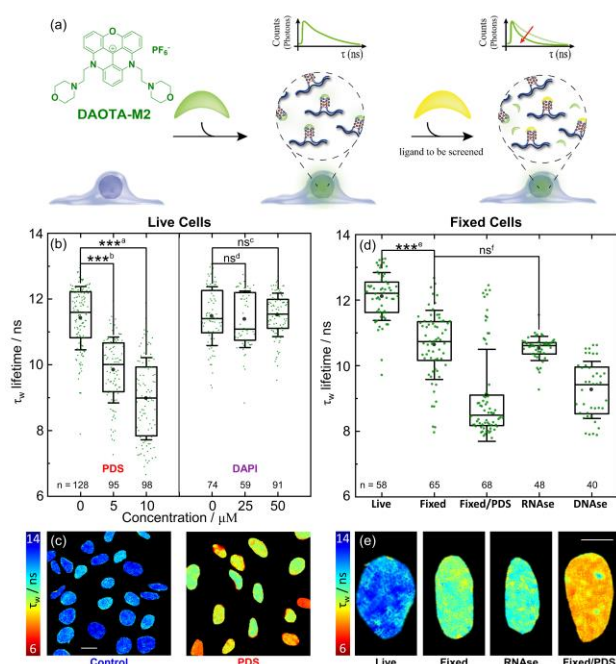
Figure 3. FLIM analysis of live and fixed U2OS cells using **DAOTA-M2**. (a) Schematic representation of the fluorescence lifetime displacement assay. Upon binding of competitors, **DAOTA-M2** is displaced from G4 to a dsDNA environment, causing a reduction in its fluorescence lifetime. (b) Box plot of mean nuclear lifetimes (τ_w) and conditions of co-incubation of **DAOTA-M2** (20 µM, 24-30 h) with PDS (24 h) and DAPI (1 h) in live cells. (c) Representative FLIM maps from **DAOTA-M2** following co-incubation with no additive (Control), and PDS (10 uM, 24 h) recorded at 256 x 256 resolution. Scale bar: 20 µm. (d) Box plot of mean nuclear lifetimes (τ_w) after fixation with PFA (4% in PBS) and treatment with PDS (10 uM, 1 h), RNAse (1 mg ml^{-1}, 10 min, 21°C) and DNAse. (200 Units well^{-1}, 1 h, 37°C). (e) Representative FLIM maps of cells from (d) recorded at 512 x 512 resolution. Scale bar: 10 µm. Results of two independent repeats. Significance: ns p > 0.05, * p < 0.05, ** p < 0.01, *** p < 0.001. [a] p = 1.8 x 10^{-36}, t = 16.1, DF = 177: [b] p = 8.7 x 10^{-25}, t = 11.8, DF = 198: [c] p = 0.75, t = −0.31, DF = 131: [d] p = 0.54, t = 0.62, DF = 126: [e] p = 3.2 x 10^{-15}, t = 9.1, DF = 114: [f] p = 0.44, t = 0.77, DF = 74.

FLIM with DAOTA-M2 in *FancJ* deficient, and *FancJ* knock-down cells. As a demonstration of how **DAOTA-M2** can be used to investigate the dynamics of G4 DNA inside live cells, we chose to investigate the role of DNA helicase *FancJ* [Figure 4], which is proposed to be involved in the resolution of G4s *in vivo*.[46] *FancJ* is known to unwind G4s *in vitro*[47] and cells lacking this protein present with general DNA replication stress, proposed to be related to the persistence of G4s.[48] Its loss of function leads to deletion of G-rich tracts and facilitates the uncoupling of DNA synthesis and histone recycling during DNA replication. Recently, *FancJ*-null mice have been described as tumour prone with enhanced predisposition

for lymphoma, and derived *FancJ*-deficient cells showed sensitivity to G4-stabilising drugs.[48,49]

To study the role of *FancJ* in altering the general G4 content *in cellulo*, we used mutant mouse embryonic fibroblast (MEF) cells in which the *FancJ* gene is compromised by a gene trap cassette, eliminating expression of the *FancJ* ORF, resulting in a null allele [Figure 4(d)].[43] Wild type MEF cells have an average nuclear lifetime of 7.9 ± 0.8 ns. Lifetimes recorded in *FancJ* mutant MEF cells showed an increase in the mean lifetime [9.6 ± 1.1 ns]. In the absence of *FancJ* helicase protein levels, the longer lifetimes suggest an increase in the stability and/or number of G4s, directly confirming the role of *FancJ* in resolving G4 structures *in cellulo*.

To corroborate this finding, its human homolog was studied in U2OS cells transfected with *FancJ* siRNA to achieve knock-down, alongside control cells transfected with siRNA against luciferase [Figure 4(e) and S6]. Cells where *FancJ* expression was knocked-down showed longer lifetimes [$\tau_w = 11.1 \pm 0.7$ ns], compared to control cells [$\tau_w = 10.5 \pm 0.7$ ns].

FancJ deficient cells, especially knock-out MEF cells, can present a DNA damage response (DDR) identified by γH2AX foci formation.[49] However, U2OS knock-down cells only activate DDR when the cells are challenged with G4 stabilisers such as Telomestatin.[47] To control for the potential indirect influence of DNA damage on **DAOTA-M2** lifetime caused by reduced *FancJ* expression, we induced DNA double strand breaks in both U2OS and MEF (wilde type and mutant) cells with 2Gy gamma irradiation. In each cell line, irradiation (and therefore nuclear DNA damage), has a very limited effect on the **DAOTA-M2** lifetime compared to those observed after *FancJ* disruption [Figure 4(b)]. We are confident that the observed variations in **DAOTA-M2** lifetimes are caused the reduction of helicase activity, and not the results of DNA damage.

These results demonstrate the potential for **DAOTA-M2** to be used directly to monitor the role of cellular G4 DNA in live cells without affecting cells through fixation or co-incubation. Moreover, these *in cellulo* experiments informed us of the specificity of **DAOTA-M2** to changes in the dynamic of G4 formation/resolution independent of DNA damage induction and give the most direct evidence to-date for the role of *FancJ* in resolving G4s in mammalian cells.
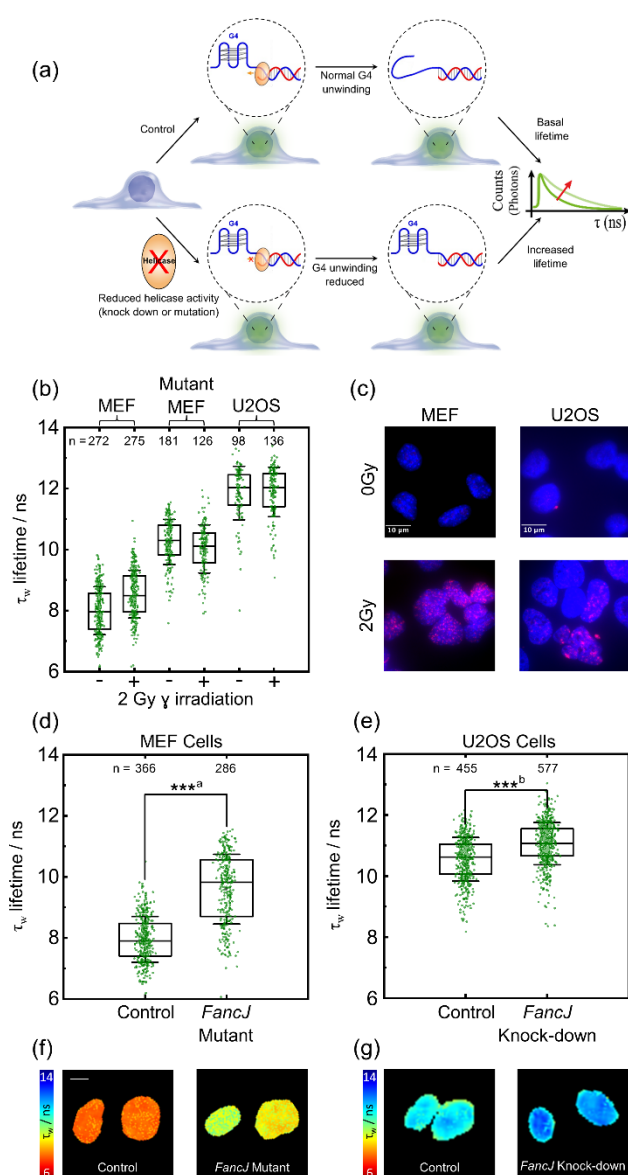

Figure 4. FLIM analysis of *FancJ* in mutant (*FancJ* abolished) MEF and knock-down (*FancJ* expression deficient) U2OS cells and using **DAOTA-M2**. (a) Schematic showing how reduced *FancJ* activity results in longer **DAOTA-M2** lifetimes. (b) Box plot of mean nuclear lifetimes (τ_w) for wild type and *FancJ* mutant MEF cells and wild type U2OS cells (incubated with **DAOTA-M2**) alongside equivalent cells exposed to 2Gy gamma irradiation. Results of 1 experiment. (c) γH2AX immunostaining (red) of wild type MEF and U2OS cells, with/without 2Gy gamma irradiation. Cells were fixed, permeabilised and

stained with γH2AX to reveal the dsDNA breaks resulting from gamma irradiation. DAPI in blue. (d) Box plot of mean nuclear lifetimes ($τ_w$) for *FancJ* wild type (control) and mutant (*FancJ* expression abolished) MEF cells. Results of two independent repeats. (e) Box plot of mean nuclear lifetimes ($τ_w$) for U2OS cells transfected with siLucif (control), or *FancJ* siRNA to knock-down *FancJ* activity. Results of two independent repeats. (f) and (g) Representative FLIM maps of cells from (d) and (e), respectively, recorded at 256 x 256 resolution. Scale bar: 10 μm. Significance: ns p > 0.05, * p < 0.05, ** p < 0.01, *** p < 0.001. [a] $p = 1.1 \times 10^{-69}$, $t = -21.1$, DF = 467. [b] $p = 2.7 \times 10^{-26}$, $t = -11.6$, DF = 959.

***In cellulo* Fluorescence Lifetime Displacement Assay.** G4s are considered as potential drug targets, and therefore it would be extremely useful to assess the ability of any given G4 targeted pharmaceutical to bind to this structure. Currently, a gold standard is to assess G4 DNA binders *in vitro,* with crucial information on whether they also target G4s in live cells missing. Our next aim was to develop a Fluorescent Lifetime Indicator Displacement Assay (FLIDA), to investigate a range of G4 binders on their ability to displace **DAOTA-M2** from live cells, as monitored by FLIM. As our test dataset, we chose the Cu/Ni/VO/Zn salphen complexes described in the *in vitro* studies (see above) since they are structurally realted but have different G4 affinities [Figure 2(g)]. All cell cultures incubated with potential G4 binders showed good viability at 1 μM over 24 hr, well beyond the 7 hr time scale of our study [Figure S7].

In cellulo FLIDA using Ni-salphen resulted in a rapid drop in lifetime over 2 hr to 8.9 ± 0.7 ns, and after 6 hr the lifetime had reached 8.1 ± 0.6 ns [Figure 5(a), orange trace], consistent with PDS [Figure 5(a), black trace]. For Zn-salphen – which has been previously shown not to interact with G4s *in vitro*[42] – no **DAOTA-M2** displacement in live cells could be detected as the lifetime remains constant [Figure 5(a), grey trace]. Both Cu and VO-salphen complexes display intermediate behaviour with lifetimes that plateau at *ca.* 10 ns after 2 h [Figures 5(a) and S8]. For Ni, VO and Zn-salphens, the *in vitro* trend [Figure 1(g)] is replicated *in cellulo* [Figure 5], correlating with the binding affinity of each complex for G4.[40-42] Cu-salphen, a strong G4 binder, did not show the magnitude of lifetime change expected from *in vitro* data,

a possible consequence of lower cellular or nuclear uptake. Thus, it appears that dynamic measurements enabled by FLIDA in live cells offer significant advantages in monitoring the ability of potential G4 binders to target G4 structures.
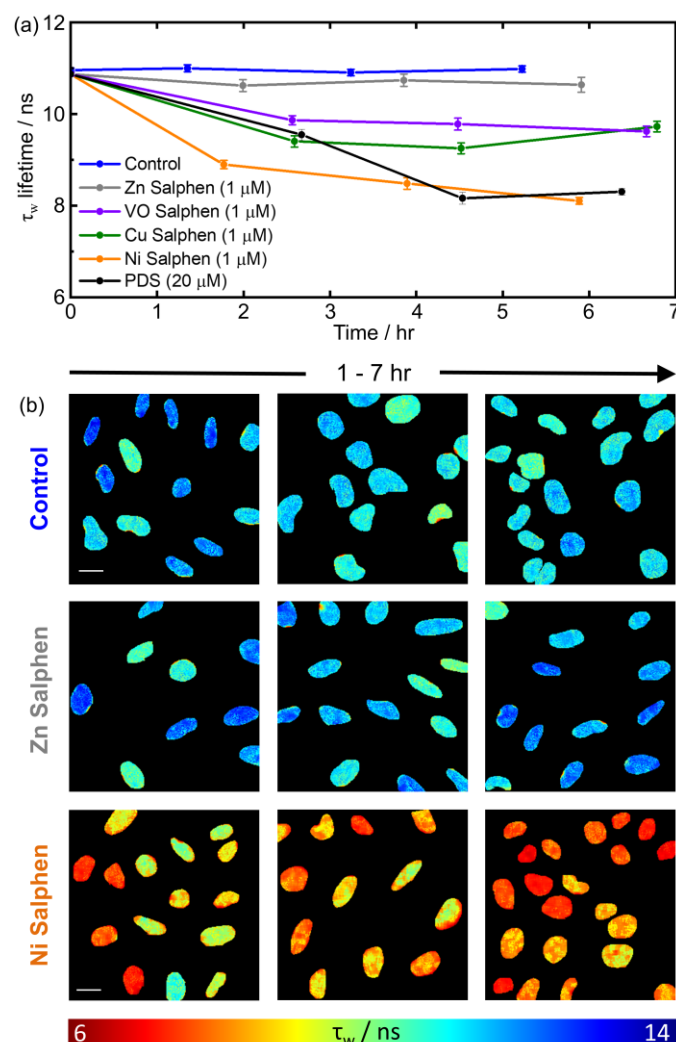

Figure 5. FLIDA with the addition of different G4 binding compounds. (a) Mean nuclear **DAOTA-M2** lifetime (τ_w) of U2OS cells during incubation with G4 binders, error bars are ± standard error of mean across two independent repeats. (b) Representative FLIM maps from (d) of the **DAOTA-M2** emission (recorded at 256 x 256 resolution), following co-incubation with DMSO (Control), Zn-salphen, Ni-salphen, and PDS. See Figure S8 for reprentative image during VO, Cu-salphen and PDS incubation. Scale bar: 20 µm.

DISCUSSION

It is becoming increasingly evident that G4 DNA structures form *in vivo* and play important biological roles. However, to date it has been difficult to visualise these structures in real time and in live cells. Based on our studies herein using FLIM with the optical probe **DAOTA-M2**,

we have been able to establish a robust displacement assay (FLIDA) to quantitatively study the interaction of any molecule with G4 DNA *in vitro* and in live cells. The advantage of our new displacement assay as compared to others previously reported, is that it is based on fluorescence lifetime rather than fluorescence intensity, which means the analysis is not dependent on concentrations and hence can be easily applied to a cellular environment. To achieve this, it was necessary to first confirm that other biomolecules present in cells would not interfere with the ability of **DAOTA-M2** to differentiate different DNA topologies. The fluorescence lifetime of our probe in nucleic acid-depleted egg extracts supplemented with G4 or dsDNA are consistent with those in aqueous buffer. Additionally, we have shown that RNA does not contribute to the **DAOTA-M2** lifetime, through digestion of RNA in fixed cells. This was of importance given the overlap in *in vitro* lifetimes when **DAOTA-M2** binds to non-G4 RNA, and G4 structures. In live cells, the average nuclear lifetimes is *ca.* 11.0 ns, which drops to *ca.* 8.5 on displacement using PDS (10 µM, 24 h), a highly specific G4 binder. Given our extensive characterisation in buffered aqueous solutions, in extract and in fixed cells, this apparent drop in nuclear lifetime was assigned to the displacement of **DAOTA-M2** from G4. In general, the lifetime values *in cellulo* are slightly higher than those from buffered and extract solutions. We attribute this difference to the change in physical and experimental conditions between bulk measurements *in vitro* and FLIM decays *in cellulo* (see experimental section). What is more important than the absolute lifetime value (which can be affected by physical parameters such as refractive index), is the relative lifetime change between a control set of cells and those where the G4 structures have been disrupted.

To establish the validity of the cellular FLIDA assays, we carried out experiments with a series of structurally related metal complexes (the metal salphens, with M = Cu, Ni, VO, Zn). As indicated above, there is a clear structure-activity relationship between the *in vitro* binding affinities and the live cell FLIDA experiments. As a further negative control we carried out

FLIDA in live cells with DAPI, which localised in the nucleus (and bound to DNA) but did not change the nuclear τ_w of **DAOTA-M2**, consistent with DAPI not displacing the probe from G4 DNA.

Interestingly, cell fixation using PFA decreased the **DAOTA-M2** lifetime which implies a difference in the nuclear G4 topology upon fixation (with a reduction in number of G4 sites available for binding with **DAOTA-M2**), a result that has not been observed previously. The FLIDA could be repeated in fixed cells using PDS, with displacement occurring to the same lifetime value as in live cells.

Having established how **DAOTA-M2** interacts with G4 DNA using known G4 binders, we next designed experiments in which the cellular dynamics of the cell are disturbed to increase the number of nuclear G4. To achieve this, we reduced helicase enzyme expression in live cells through knock-down and knock-out of *FancJ,* in U2OS and in MEF cells, respectively. For the first time in live mammalian cells, we show directly that reducing G4 helicase activity increases the number and/or stability of G4s as nuclear lifetime increases. In U2OS cells, the increased lifetimes when *FancJ* expression is knocked-down is relatively small (0.5 ns), when compared to the decrease in lifetime after PDS displacement (*ca.* 2.5 ns). This is expected, given that this helicase transiently targets specific regions of the genome and probably acts only on a proportion of the cellular G4 content inside each cell. Similarly to human cells, the mutation of *FancJ* in mouse cells results in an increase in G4 lifetime of 1.7 ns, larger than the knock-down in U2OS (0.5 ns). We also noticed that MEF cells have a lower baseline average nuclear lifetime compared to U2OS (*ca.* 8 ns and *ca.* 11 ns, respectively). ALT positive U2OS human cells are deficient for ATRX;[50] a known G4 binder, the down-regulation of which is associated to increased stability of G4.[51] It is possible that the genetic background of U2OS is responsible for the difference in lifetime with MEF cells that are proficient for ATRX. DNA helicase knock-downs have multiple cellular and molecular effects on the genome, transcriptome and

RNA trafficking,[52-54] including the possibility of forming ssDNA, double-strand breaks and affecting RNA molecules. Treatment with cisplatin showed a slight increase in nuclear lifetime, indicating that intrastrand DNA adducts and interstrand crosslinks can result in a shift in **DAOTA-M2** lifetime [Figure S5]. However, our previous *in vitro* work using short chain oligonucleotides suggests that exposed dsDNA ends do not lead to increased fluorescence lifetime,[30] and dsDNA breaks induced by gamma irradiation had minimal effect on the **DAOTA-M2** lifetime. Given this result, it is very unlikely that the significant increase in lifetime measurements observed in the *FancJ* knock-down and mutant experiments reflects an increase in binding of **DAOTA-M2** to other DNA structures that might form in these genetic backgrounds. With these factors accounted for, we can say with confidence that FLIM analysis of **DAOTA-M2** has revealed directly the critical role of DNA helicase *FancJ* in unwinding G4 in live mammalian cells.

G4 DNA targeting is emerging as a novel design strategy in the development of therapeutic drugs for diseases such as cancer,[55] thus, a robust method to test their G4 binding in live cells is highly desirable. We have demonstrated that **DAOTA-M2** can be used to investigate G4 dynamics and their interaction with G4 binders *in cellulo* in real time. This approach holds great promise for monitoring the sensitivity of newly developed G4 targeting drugs (*e.g.* testing against various cancer cell lines, including patient derived samples) as well as for further understanding of the *in vivo* role of G4 DNA.

Conclusions

We have used **DAOTA-M2** in combination with FLIM to unambiguously establish the formation of G4 DNA in the nuclei of live cells. We have developed a new cellular assay to study the interaction of small molecules with G4 DNA, which can be applied to a wide range of drugs, which do not have intrinsic fluorescence. Our finding that cell fixation has a significant effect on the **DAOTA-M2** lifetime, which must reflect a change in DNA topology, has wider implications for G4 studies that require fixations protocols. Additionally, our method can be used to study G4 DNA dynamics in live cells, for example when the expression of helicases known to unwind G4 *in vitro* is reduced or abolished. The knock-down of *FancJ* in U2OS or mutation of *FancJ* in MEF cells both increase the nuclear lifetime, consistent with a reduction in helicase enzyme activity in both cases. These experiments pave the way to directly study G4-related biological phenomena in live cells and to correlate, for the first time, the biological activity of small molecules with their ability to target G4 DNA structures in live cells.

METHODS

DAOTA-M2 and metal-salphens (Ni, Cu, VO, Zn) complexes were synthesised as previously reported.[30,41,42] PDS was kindly donated by Dr. Marco Di-Antonio, synthesised according to literature methods.[56,57] DAPI and cisplatin were purchased from commercial sources. Oligonucleotides (*c-Myc* and ds26; sequences = 5'-TGAGGGTGGGTAGGGTGGGTAA-3' and 5'-CAATCGGATCGAATTCGATCCGATTG-3', respectively) were purchased from Eurogentec, and dissolved in 10 mM lithium cacodylate buffer at pH 7.3. KCl was added to a final concentration of 100 mM, then the oligonucleotides were annealed at 95 °C for 5-10 min. Calf thymus DNA (CT-DNA, Sigma) was dissolved in the same cacodylate buffer, and KCl added to a final concentration of 100 mM. All oligonucleotide concentrations were determined unannealed using the molar extinction coefficients 13200 (base pair for CT-DNA), 228700 (strand for *c-Myc*) and 253200 (strand for ds26). Concentrations of G4 and dsDNA are expressed as per strand, and per base pair, respectively.

***In vitro* time-correlated single photon counting (TCSPC).** Time-resolved fluorescence decays were obtained using an IBH 5000F time-correlated single photon counting (TCSPC) device (Jobin Ybon, Horiba) equipped with a 467 nm NanoLED as an excitation source (pulse width < 200 ps, HORIBA) with a 100 ns time window and 4096 time bins. Decays were detected at λ_{em} = 575 nm (± 12 nm) after passing through a 530 nm long pass filter to remove any scattered excitation pulse. For experiments using Ni-, Cu- or VO-salphens, a 404 nm NanoLED excitation source was used. For experiments experiments involving ≤ 0.2 µM **DAOTA-M2**, 256 time bins were used detected at λ_{em} = 575 nm (± 16 nm) to increase signal intensity per bin. Decays were accumulated to 10000 counts. A neutral density filter was used for the instrument response function (IRF) measurements using a *Ludox* solution, detecting the emission at the excitation wavelength. Traces were fitted by iterative reconvolution to the equation $I(t) = I_0((1-\alpha_1-\alpha_2)e^{-t/\tau 1}+\alpha_1 e^{-t/\tau 2}+\alpha_2 e^{-t/\tau 3})$ where α_1 and α_2 are variables and α is

normalised to unity. The mean-weighted fluorescence lifetime was calculated from both lifetime components (τ_i) and their amplitudes (α_i) using the equation:

$$\tau_{mean-weighted} = \frac{\tau_1^2\,\alpha_1 + \tau_2^2\,\alpha_2}{\tau_1\,\alpha_1 + \tau_2\,\alpha_2} \qquad (1)$$

A prompt shift was included in the fitting to take into account differences in the emission wavelength between the IRF and measured decay. The goodness of fit was judged by consideration of the deviations from the model *via* a weighted residuals plot. Least square minimization was performed using the Quasi-Newton algorithm.

***In vitro* fluorescence lifetime displacement assay. DAOTA-M2** (2 µM) was dissolved in 10 mM lithium cacodylate buffer (pH 7.3) supplemented with 100 mM KCl and the time-resolved fluorescence decay was recorded. If needed, dsDNA (CT-DNA, 20 µM) was mixed with **DAOTA-M2** and the decay recorded. Pre-folded G4 DNA (*c-Myc*, 4 µM) was then added and the decay recorded. Increasing amounts of the corresponding molecules under study were added and the fluorescence decay recorded until no further changes were observed.

***In vitro* fluorescence lifetime measurements with nucleic acid-depleted egg extracts.** Decay data for nucleic acid-depleted cell extract studies was acquired by mixing 33 µL of nucleic acid-depleted *Xenopus Laevis* egg extracts,[36] with 12 µL of 10 mM lithium cacodylate buffer (pH 7.3) containing 100 mM KCl, **DAOTA-M2** (final concentration 2 µM) and oligonucleotide (final concentration: *c-Myc* = 4 µM or ds26 = 44 µM). For samples where cell extract was not used, the same volume of 10 mM lithium cacodylate buffer (pH 7.3) containing 100 mM KCl was used in its place. Lifetimes decays were recorded using a home-built TCSPC method described previously.[58] Samples were excited using a pulsed diode laser (Becker & Hickl GmbH, 477 nm, 20 MHz) and emission collected at 575 nm (± 15 nm), using a 550 nm long pass filter to remove scattered excitation photons. Decay traces were fitted using the FLIMfit software tool developed at Imperial College London (v5.1.1, Sean Warren, Imperial

College London) to a bi-exponential function, and the mean weighted lifetime (τ_w) calculated using equation (1).

General cell culture. Human Bone Osteosarcoma Epithelial Cells (U2OS, from ATCC) were grown in high glucose Dulbecco's modified Eagle medium (DMEM) containing 10% fetal bovine serum at 37 °C with 5% CO_2 in humidified air.

In cellulo **fluorescence lifetime displacement assay**. Cells were seeded on chambered coverglass (1.5×10^4 cells, 250 μl, 0.8 cm^2) for 24 h, before washing with Phosphate-Buffered Saline (PBS) and adding fresh media containing **DAOTA-M2** (20 μM, 250 μl) for a further 24h. For 24 hr co-incubation experiments, the compound under study was added with **DAOTA-M2** and imaged 24 hr later. For < 24 hr co-incubation experiments, the compound udder study was added directly to the incubation media after 24 hr **DAOTA-M2** incubation, and images taken over time. Cells were imaged directly in the final incubation media.

Fixed Cell experiments. Cells were seeded on chambered coverglass (1.5×10^4 cells, 250 μl, 0.8 cm^2) for 24 h, before washing with PBS and adding fresh media containing **DAOTA-M2** (20 μM, 250 μl) for a further 24h. Cells were washed (x3) in ice cold PBS before incubation in ice cold paraformaldehyde (PFA, 4% in PBS) solution for 10 min at 21°C, and a further wash (x3) with ice cold PBS. Fixed cells were further treated with PDS (10 uM, 1 hr, 21°C), RNAse A (1 mg ml^{-1}, 10 min, 21°C, Merck) or DNAse (200 Units well^{-1}, 1 hr, 37°C, Qiagen), and left under PBS.

Cell culture for helicase knock-down and knock-out experiments. For *FancJ* helicase knock-down treatment, a solution of 30 nM siRNA (SigmaAldrich, 5'-GUACAGUACCCCACCUUAU -3') and DharmaFECT reagent (used as per manufacturer's instructions, Dharmacon) in serum-free DMEM was prepared and incubated at RT for 30 min. 400 μL of this solution was mixed with 2.1 mL DMEM containing 10% FBS and used to seed

cells (1.6×10^5 cells, 2.50 ml, 9.6 cm^2) for 16 hr at 37°C. The growth medium was replenished, and cells further incubated for 24h before reseeding on chambered coverglass (5.0×10^4 cells, 400 µl, 0.8 cm^2) with addition of **DAOTA-M2** (10 µM) for a further 24 hr before imaging. Cells treated analogously using an siRNA for Luciferase (Dharmacon, 5'-UCGAAGUAUUCCGCGUACG -3') were used as a control. The knockdown efficiency was assessed by Western blot for *FancJ* compared to actin [Figure S6].

FancJ $^{+/-}$ and *FancJ* $^{-/-}$ Mouse Embryonic Fibroblast cells (a kind gift from S. Boulton) were cultured as described above for U2OS cells. For FLIM, cells were reseeded on chambered coverglass ($1.5-5 \times 10^4$ cells, 200 µl, 0.8 cm^2) for 24-48 hr in media, incubated with **DAOTA-M2** (20 µM) for 24 hr before imaging.

Cytoxicity assay. U2OS cells were seeded (5×10^3 cells, 100 µl, 32.2 mm^2) in a 96-well plate. After 24 h, compounds under study were added at the appropriate concentration in triplicate (150 µl). After a further 24 h, 20 µl of the MTS Assay reagent was added according to the Promega MTS Assay protocol. The average absorbance of the triplicate wells was recorded at 492 nm, 12 hr after reagent addition. Cell treatments were corrected for compound absorbance by subtracting the compound-only control run in parallel. Absolute IC$_{50}$ was determined from the dose response curve of absorbance *vs.* logarithm of concentration of compound. Results are expressed as mean ± SD of three independent repeats.

Fluorescence lifetime imaging microscopy (FLIM). FLIM was performed through time-correlated single-photon counting (TCSPC), using an inverted confocal laser scanning microscope (Leica, SP5 II) and a SPC-830 single-photon counting card (Becker & Hickl GmbH). A pulsed diode laser (Becker & Hickl GmbH, 477 nm, 20 MHz) was used as the excitation source, with a PMC-100-1 photomultiplier tube (Hamamatsu) detector. Fluorescence emission (550 – 700 nm) was collected through a 200 µm pinhole for an acquisition time sufficient to obtain signal strength suitable for decay fitting, or a maximum of

1000s. For all live cell imaging, cells were mounted (on chambered coverglass slides) in the microscope stage, heated by a thermostat (Lauda GmbH, E200) to 37 ($\pm$ 0.5)°C, and kept under an atmosphere of 5% CO_2 in air. A 100x (oil, NA = 1.4) or 63x (water, NA = 1.2) objective was used to collect images at either 256 x 256 pixel resolution or at 512 x 512 pixel resolution, as stated in the text. The IRF used for deconvolution was recorded using reflection of the excitation beam from a glass cover slide.

Lifetime data were fitted using the FLIMfit software tool developed at Imperial College London (v5.1.1, Sean Warren, Imperial College London) to a bi-exponential function, and the mean weighted lifetime (τ_w) calculated using equation (1). 7 x 7 and 9 x 9 square binning was used to increase signal strength for images recorded at 256 x 256 and 512 x 512 resolution, respectivly. A scatter parameter was added to the decay fitting to account for scattered excitation light. Before fitting, a mask was applied to the images to analyse individual cell nuclei. Fitted lifetime data for each pixel within a single cell nucleus were pooled to find average and median nuclear τ_w values. A threshold was applied to the average of each nucleus to require a minimum of 300 at the peak of the decay and a goodness-of-fit measured by χ^2 of less than 2. Average nuclear intensity in FLIM images was calculated from the maximum of the fitted decay (excluding scatter), averaged across the nucleus.

Gamma irradiation. Chamber slides containing either U2OS or MEF cells were inserted into the Irradiator (GSR D1 Cell Irradiator) for 50 s to irradiate cells to 2 Gy. Control cells were left outside for the equivalent time. Samples for FLIM were then imaged as above. To confirm DNA damage, slides were further incubated for 30 min to allow initiation of damage repair by the cells. Then, cells were permeabilised with Triton X-100 buffer (0.5% Triton X-100; 20 mM Tris pH 8; 50 mM NaCl; 3 mM $MgCl_2$; 300 mM sucrose) at RT for 5 min and then fixed in 3% formaldehyde/2% sucrose in PBS for 15 min at RT and washed with PBS (x3). After a 10 min permeabilisation step and a wash in PBS, nuclei were incubated with blocking solution (10%

goat serum in PBS) for 30 min at 37°C and stained with mouse-anti-gH2AX (1/500, Millipore 05-636) for 1 hr at 37°C followed by O/N incubation at 4°C. After washing in PBS (x3), slides were incubated with secondary goat anti-mouse Alexa 488 antibody (1/400, Life Technologies A11001) for 40 min at 37°C, washed in PBS (x3), post fixed for 10 min and incubated with ethanol series (70%, 80%, 90%, 100%). Slides were mounted with antifade reagent (ProLong Gold, Invitrogen) containing DAPI and images were captured with Zeiss microscope using Carl Zeiss software.

Western Blot. Protein was extracted from cells using a lysis buffer (40 mM NaCl, 25 mM Tris pH 8, 2 mM $MgCl_2$, 0.05% SDS, 2x Complete EDTA-free protease inhibitor (Roche), 0.4 $\mu L \ mL^{-1}$ benzonase) with protein concentration determined by Bradford assay, comparing to BSA standards to ensure loading of an equal mass of protein into each lane. Protein and Laemmli buffer were heated to 100°C for 5 min before loading into NuPAGE Novex 4%–12% Bis-Tris Gel (Invitrogen). Samples were run on gels for 2 hr before transfer from gel to a nitrocellulose membrane. Antibodies used to bind proteins on membrane were pAb rabbit BRIP1/FANCJ antibody (1/10000, Novus Biologicals NBP1-31883) and mAb mouse anti-β-actin antibody (1/5000, Abcam ab8226). Secondary antibodies used were: pAb swine anti-rabbit immunoglobulins/HRP (1/10000, Dako P0217) and pAb goat anti-mouse immunoglobulins/HRP (1/5000, invitrogen A16078). Visualisation was performed by exposure onto photographic film.

Statistics. Results are expressed as mean ± SD (unless stated otherwise). Two-tailed non-paired t-tests were performed using OriginPro 9.55. p-values, t-values and degrees of freedom (DF) are stated in the figure captions. Significance: ns $p > 0.05$, * $p < 0.05$, ** $p < 0.01$, *** $p < 0.001$. n values are the total cell nuclei that meet the threshold requirements. For box

plots, the box represents 25%-75% range, error bars are the mean ± SD, horizontal line is the median and the grey dot is the mean.

Acknowledgements

Author contributions

P.A.S., B.L., J.G.-G., J.B.V, M.K.K. and R.V. designed the study and co-wrote the paper. P.A.S., B.L., J.G.-G. performed experiments and analysed the data. N.M.-P. provided nucleic acid-free extracts and advised on the design of the corresponding experiments. A.L. and D.M. performed the cytotoxicity studies. J.B.E. and P.C. provided advice in the design of the experiments and analysis of the FLIM data. R.M.P. performed DNA damage response staining (gH2AX) and analysis.

References

1   Neidle, S. Quadruplex nucleic acids as targets for anticancer therapeutics. *Nat. Rev. Chem.* **1**, 10 (2017).

2   Murat, P. & Balasubramanian, S. Existence and consequences of G-quadruplex structures in DNA. *Curr. Opin. Genet. Dev.* **25**, 22-29 (2014).

3   Rhodes, D. & Lipps, H. J. G-quadruplexes and their regulatory roles in biology. *Nucleic Acids Res.* **43**, 8627-8637 (2015).

4   Bochman, M. L., Paeschke, K. & Zakian, V. A. DNA secondary structures: stability and function of G-quadruplex structures. *Nat. Rev. Genet.* **13**, 770-780 (2012).

5   Huppert, J. L. & Balasubramanian, S. Prevalence of quadruplexes in the human genome. *Nucleic Acids Res.* **33**, 2908-2916 (2005).

6   Todd, A. K., Johnston, M. & Neidle, S. Highly prevalent putative quadruplex sequence motifs in human DNA. *Nucleic Acids Res.* **33**, 2901-2907 (2005).

7   Bedrat, A., Lacroix, L. & Mergny, J. L. Re-evaluation of G-quadruplex propensity with G4Hunter. *Nucleic Acids Res.* **44**, 1746-1759 (2016).

8   Chambers, V. S. *et al.* High-throughput sequencing of DNA G-quadruplex structures in the human genome. *Nat. Biotechnol.* **33**, 877-881 (2015).

9   Hansel-Hertsch, R. *et al.* G-quadruplex structures mark human regulatory chromatin. *Nat. Genet.* **48**, 1267-1272 (2016).

10   Hänsel-Hertsch, R., Spiegel, J., Marsico, G., Tannahill, D. & Balasubramanian, S. Genome-wide mapping of endogenous G-quadruplex DNA structures by chromatin immunoprecipitation and high-throughput sequencing. *Nat. Protoc.* **13**, 551-564 (2018).

11   Fouquerel, E., Parikh, D. & Opresko, P. DNA damage processing at telomeres: The ends justify the means. *DNA Repair* **44**, 159-168 (2016).

12   De Magis, A. *et al.* DNA damage and genome instability by G-quadruplex ligands are mediated by R loops in human cancer cells. *Proc. Natl. Acad. Sci. U. S. A.* **116**, 816-825 (2019).

13   Mendoza, O., Bourdoncle, A., Boule, J. B., Brosh, R. M. & Mergny, J. L. G-quadruplexes and helicases. *Nucleic Acids Res.* **44**, 1989-2006 (2016).

14   Brown, B. A. *et al.* Isolation and characterization of a monoclonal anti-quadruplex DNA antibody from autoimmune "viable motheaten" mice. *Biochemistry* **37**, 16325-16337 (1998).

15   Schaffitzel, C. *et al.* In vitro generated antibodies specific for telomeric guanine-quadruplex DNA react with Stylonychia lemnae macronuclei. *Proc. Natl. Acad. Sci. U. S. A.* **98**, 8572-8577 (2001).

16   Biffi, G., Tannahill, D., McCafferty, J. & Balasubramanian, S. Quantitative visualization of DNA G-quadruplex structures in human cells. *Nature Chem.* **5**, 182-186 (2013).

17   Biffi, G., Di Antonio, M., Tannahill, D. & Balasubramanian, S. Visualization and selective chemical targeting of RNA G-quadruplex structures in the cytoplasm of human cells. *Nature Chem.* **6**, 75-80 (2014).

18   Liu, H. Y. *et al.* Conformation selective antibody enables genome profiling and leads to discovery of parallel G-quadruplex in human telomeres. *Cell Chem. Biol.* **23**, 1261-1270 (2016).

19   Douglas, M. P. & Rogers, S. O. DNA damage caused by common cytological fixatives. *Mutat. Res., Fundam. Mol. Mech. Mutagen.* **401**, 77-88 (1998).

20   Srinivasan, M., Sedmak, D. & Jewell, S. Effect of fixatives and tissue processing on the content and integrity of nucleic acids. *Am. J. Pathol.* **161**, 1961-1971 (2002).

21   Chilka, P., Desai, N. & Datta, B. Small molecule fluorescent probes for G-quadruplex visualization as potential cancer theranostic agents. *Molecules* **24** (2019).

22   Pandith, A., Siddappa, R. G. & Seo, Y. J. Recent developments in novel blue/green/red/NIR small fluorescent probes for in cellulo tracking of RNA/DNA G-quadruplexes. *J. Photochem. Photobiol., C* **40**, 81-116 (2019).

23   Monchaud, D. Quadruplex detection in human cells. Preprint at https://arxiv.org/abs/1910.07023 (2019).

24   Mohanty, J. *et al.* Thioflavin T as an efficient inducer and selective fluorescent sensor for the human telomeric G-quadruplex DNA. *J. Am. Chem. Soc.* **135**, 367-376 (2013).

25   Xu, S. J. *et al.* Thioflavin T as an efficient fluorescence sensor for selective recognition of RNA G-quadruplexes. *Sci. Rep.* **6** (2016).

26   Guan, A. J. *et al.* Ethyl-substitutive Thioflavin T as a highly-specific fluorescence probe for detecting G-quadruplex structure. *Sci. Rep.* **8** (2018).

27   Xue, C., Lin, T. Y. W., Chang, D. & Guo, Z. F. Thioflavin T as an amyloid dye: fibril quantification, optimal concentration and effect on aggregation. *R. Soc. open sci.* **4** (2017).

28   Stsiapura, V. I. *et al.* Thioflavin T as a molecular rotor: fluorescent properties of Thioflavin T in solvents with different viscosity. *J. Phys. Chem. B* **112**, 15893-15902 (2008).

29   Rajput, C., Rutkaite, R., Swanson, L., Haq, I. & Thomas, J. A. Dinuclear monointercalating Ru-II complexes that display high affinity binding to duplex and quadruplex DNA. *Chem.: Eur. J.* **12**, 4611-4619 (2006).

30   Shivalingam, A. *et al.* The interactions between a small molecule and G-quadruplexes are visualized by fluorescence lifetime imaging microscopy. *Nat. Commun.* **6**, 8178 (2015).

31   Tseng, T. Y. *et al.* The G-quadruplex fluorescent probe 3,6-bis(1-methyl-2-vinyl-pyridinium) carbazole diiodide as a biosensor for human cancers. *Sci. Rep.* **8** (2018).

32   Tseng, T. Y., Chu, I. T., Lin, S. J., Li, J. & Chang, T. C. Binding of small molecules to G-quadruplex DNA in cells revealed by fluorescence lifetime imaging microscopy of o-BMVC foci. *Molecules* **24** (2019).

33   Liu, L.-Y. *et al.* Content detection of G-Quadruplex DNA in live cells based on photon counts and complex structures. *Angew. Chem.*, 10.1002/ange.202002422 (2020).

34   Kotar, A. *et al.* NMR structure of a triangulenium-based long-lived fluorescence probe bound to a G-Quadruplex. *Angew. Chem.-Int. Edit.* **55**, 12508-12511 (2016).

35   Shivalingam, A. *et al.* Trianguleniums as optical probes for G-Quadruplexes: A photophysical, electrochemical, and computational study. *Chem.: Eur. J.* **22**, 4129-4139 (2016).

36   Hoogenboom, W. S., Klein Douwel, D. & Knipscheer, P. Xenopus egg extract: a powerful tool to study genome maintenance mechanisms. *Dev. Biol.* **428**, 300-309 (2017).

37   Koirala, D. *et al.* A single-molecule platform for investigation of interactions between G-quadruplexes and small-molecule ligands. *Nature Chem.* **3**, 782-787 (2011).

38   Le, D. D., Di Antonio, M., Chan, L. K. M. & Balasubramanian, S. G-quadruplex ligands exhibit differential G-tetrad selectivity. *Chem. Commun. (Cambridge, U. K.)* **51**, 8048-8050 (2015).

39   Tanious, F. A., Veal, J. M., Buczak, H., Ratmeyer, L. S. & Wilson, W. D. DAPI (4',6-diamidino-2-phenylindole) binds differently to DNA and RNA - Minor-groove binding at AT sites and intercalation at AU sites. *Biochemistry* **31**, 3103-3112 (1992).

40   Campbell, N. H. *et al.* Molecular basis of structure-activity relationships between salphen metal complexes and human telomeric DNA quadruplexes. *J. Med. Chem.* **55**, 209-222 (2012).

41   Reed, J. E., Arnal, A. A., Neidle, S. & Vilar, R. Stabilization of G-quadruplex DNA and inhibition of telomerase activity by square-planar nickel(II) complexes. *J. Am. Chem. Soc.* **128**, 5992-5993 (2006).

42   Arola-Arnal, A., Benet-Buchholz, J., Neidle, S. & Vilar, R. Effects of metal coordination geometry on stabilization of human telomeric quadruplex DNA by square-planar and square-pyramidal metal complexes. *Inorg. Chem.* **47**, 11910-11919 (2008).

43   Abd Karim, N. H. *et al.* Salphen metal complexes as tunable G-quadruplex binders and optical probes. *RSC Adv.* **4**, 3355-3363 (2014).

44   Rodriguez, R. *et al.* Small-molecule-induced DNA damage identifies alternative DNA structures in human genes. *Nat. Chem. Biol.* **8**, 301-310 (2012).

45   Shen, D. W., Pouliot, L. M., Hall, M. D. & Gottesman, M. M. Cisplatin resistance: a cellular self-defense mechanism resulting from multiple epigenetic and genetic changes. *Pharmacol. Rev.* **64**, 706-721 (2012).

46   Leon-Ortiz, A. M., Svendsen, J. & Boulton, S. J. Metabolism of DNA secondary structures at the eukaryotic replication fork. *DNA Repair* **19**, 152-162 (2014).

47   Wu, Y. L., Shin-ya, K. & Brosh, R. M. FANCJ helicase defective in Fanconia anemia and breast cancer unwinds G-quadruplex DNA to defend genomic stability. *Mol. Cell. Biol.* **28**, 4116-4128 (2008).

48   Sarkies, P. *et al.* FANCJ coordinates two pathways that maintain epigenetic stability at G-quadruplex DNA. *Nucleic Acids Res.* **40**, 1485-1498 (2012).

49   Matsuzaki, K., Borel, V., Adelman, C. A., Schindler, D. & Boulton, S. J. FANCJ suppresses microsatellite instability and lymphomagenesis independent of the Fanconi anemia pathway. *Genes Dev.* **29**, 2532-2546 (2015).

50   Lovejoy, C. A. *et al.* Loss of ATRX, genome instability, and an altered DNA damage response are hallmarks of the alternative lengthening of telomeres pathway. *PLoS Genet.* **8** (2012).

51   Wang, Y. X. *et al.* G-quadruplex DNA drives genomic instability and represents a targetable molecular abnormality in ATRX-deficient malignant glioma. *Nat. Commun.* **10** (2019).

52   Vannier, J. B. *et al.* RTEL1 Is a replisome-associated helicase that promotes telomere and genome-wide replication. *Science* **342**, 239-242 (2013).

53   Schertzer, M. *et al.* Human regulator of telomere elongation helicase 1 (RTEL1) is required for the nuclear and cytoplasmic trafficking of pre-U2 RNA. *Nucleic Acids Res.* **43**, 1834-1847 (2015).

54   Bharti, S. K., Awate, S., Banerjee, T. & Brosh, R. M. Getting ready for the dance: FANCJ orons out DNA wrinkles. *Genes* **7** (2016).

55   Neidle, S. Quadruplex Nucleic Acids as Novel Therapeutic Targets. *J. Med. Chem.* **59**, 5987-6011 (2016).

56   Rodriguez, R. *et al.* A novel small molecule that alters shelterin integrity and triggers a DNA-damage response at telomeres. *J. Am. Chem. Soc.* **130**, 15758-15759 (2008).

57   Muller, S., Kumari, S., Rodriguez, R. & Balasubramanian, S. Small-molecule-mediated G-quadruplex isolation from human cells. *Nature Chem.* **2**, 1095-1098 (2010).

58   Vysniauskas, A. *et al.* Exploring viscosity, polarity and temperature sensitivity of BODIPY-based molecular rotors. *Phys. Chem. Chem. Phys.* **19**, 25252-25259 (2017).